

Towards event-by-event studies of the ultrahigh-energy cosmic-ray composition

D. S. Gorbunov^a, G. I. Rubtsov^{a,b} and S. V. Troitsky^a

^a*Institute for Nuclear Research of the Russian Academy of Sciences,
60th October Anniversary Prospect 7a, 117312, Moscow, Russia*

^b*Moscow State University, Vorobiovy Gory, Moscow, Russia*

Abstract

We suggest a method which improves the precision of studies of the primary composition of ultra-high-energy cosmic rays. Two principal ingredients of the method are (1) comparison of the observed and simulated parameters for *individual* showers, without averaging over arrival directions and (2) event-by-event selection of simulated showers by the physical observables and not by the reconstructed primary parameters. A detailed description of the algorithm is presented and illustrated by several examples.

Key words:

PACS: 98.70.Sa ultra-high-energy cosmic rays, primary composition

1 Introduction

The determination of the primary composition of cosmic rays with energies higher than $\sim 10^{17}$ eV is a real challenge. The lack of knowledge of the types of primary ultra-high-energy particles which induce extensive air showers makes it difficult to study their origin and in some cases even to determine their energy spectrum. More precise and less model-dependent determination of the cosmic-ray primary composition, especially in the highest-energy domain, is one of the most important tasks in contemporary astroparticle physics (for a review and discussions see e.g. Ref. [1]).

Ultra-high-energy cosmic rays are observed through air showers, and to extract information about the primary particle, selected observables of real air show-

Email address: st@ms2.inr.ac.ru (S. V. Troitsky).

ers are compared to those of simulated ones for different primaries. Because of large shower-to-shower fluctuations, one cannot determine the primary-particle type of an individual air shower. That is why traditional approaches to the composition studies are based on the determination of average characteristics of a large sample of cosmic-ray events. This approach has obvious advantages: for a homogeneous composition, averaging smoothens out the fluctuations, and large statistics results in higher precision. Furthermore, the computational time required to perform reliable simulations of an observable averaged over a large sample is much smaller than that necessary for detailed simulations of all events in the data set. However, for mixed composition, averaging might become a problem because fluctuations of the discriminating observables over their central values are larger when air showers from different arrival directions are combined in one sample. Different zenith angles correspond to different atmospheric depths, and air showers detected by surface arrays have different stages of development and hence may have quite different observable parameters even for the same energies and primaries. Moreover, the geomagnetic field introduces the azimuthal dependence for photon [2] and very inclined hadron [3] showers. Even fluorescent detectors, which observe the shower development on its way through the atmosphere, respond to showers from different arrival directions in different ways, notably with different accuracies. For gamma-ray primaries at $E \gtrsim 5 \cdot 10^{19}$ eV, the entire shower development is direction-dependent.

We suggest to improve considerably the precision of the composition studies by performing individual simulations for each observed high-energy event. In the case of a large number of events in a data sample, averaging in bins of arrival directions may be used. If one is not interested in the study of possible gamma-ray primaries with $E \gtrsim 5 \cdot 10^{19}$ eV, binning in zenith angle only is often sufficient.

This method, in its simplest form with one observable, has been successfully implemented to obtain a limit on the gamma-ray fraction in the primary flux at $E > 10^{20}$ eV using the data of the AGASA and Yakutsk experiments [4]. Event-by-event simulations (without selection by reconstructed parameters) were previously used for the composition studies in Refs. [5–7].

The rest of the paper is organized as follows. In Sec. 2, we present the sketch of the event-by-event approach to the composition studies, discuss the choice of the air-shower observables (Sec. 2.1), give a general idea of how to constrain the probable primary-particle type of an individual air shower (Sec. 2.2) and how to use these shower-by-shower constraints to gain information about the chemical composition of the primary cosmic-ray flux using a sample of events (Sec. 2.3). Sec. 3 contains the detailed description of the procedure outlined in Sec. 2 and ready-to-use formulae implementing this procedure. Sec. 4 presents several examples which illustrate the method by the analysis of small (and

hence statistically insignificant) samples of events. There, we consider only one composition-related observable, the muon density, and use samples of highest-energy AGASA and Yakutsk events as examples. In Sec. 4.1, we analyse in detail a single event (the highest energy air shower reported by AGASA). The procedure for estimating the limit on the fraction of particular primaries in a given energy range is illustrated in Sec. 4.2 with the sample of six AGASA showers with reported energies higher than 10^{20} eV and known muon content, while the algorithm to determine the best-fit composition assuming two possible primaries is illustrated in Sec. 4.3 with a sample of four events with reported energies above $1.5 \cdot 10^{20}$ eV detected by the AGASA and Yakutsk experiments. Both samples are small and the analysis of Sec. 4 serves for illustrative purposes only. We briefly summarize and discuss novelties of our method in Sec. 5. Some of our notations are summarized in Appendix A. Appendices B and C contain technical information related to the examples presented in Sec. 4.

2 Generalities

In this section, we sketch the main elements of our approach to study individual air-shower events and their ensembles. An operational algorithm is given in Sec. 3 and illustrated in Sec. 4.

2.1 *Two classes of observables*

On the basis of detector readings, several air-shower observables can be determined experimentally; many of them are not independent of each other. For our purposes, we separate them into two groups which we will treat differently.

2.1.1 *E-observables*

This class contains the parameters related to the energy estimation and the arrival direction. For ground arrays, E-observables usually include the signal density at a given distance from the shower core (known as $S(600)$ or $S(1000)$); for fluorescent telescopes the E-observable is the total amount of the fluorescent light (corrected for atmospheric conditions).

The arrival direction may be fixed because the pointing accuracy at high energies is often relatively high and variations of the arrival direction within the error bars have a negligible, compared to shower-to-shower fluctuations, effect on both energy estimation and measurement of the composition-related

parameters. In the case of poor angular resolution, for example for fluorescent detectors in the monocular mode, the arrival direction should be treated on the same footing as other E-parameters.

In what follows, we ignore, for simplicity, the errors in the determination of the arrival direction and consider a single E-observable — the reconstructed energy of a shower, E_{rec} . For a fixed arrival direction, E_{rec} is in one-to-one correspondence with the energy estimator used by a given experiment.

We note that E-observables are primary-dependent but this dependence is naturally accounted for in the method, see Sec. 2.2.

2.1.2 C-observables

We call the parameters used to distinguish various types of primary particles C-observables. Depending on the experiment, they may include muon density or muon richness, the slope of the lateral distribution function of the total signal or of muons only, shower front curvature, rise time etc. For a more efficient separation of different primaries, simultaneous use of several such parameters is justified, and we hereafter denote the set of these parameters as $\mathbf{c} = (c_1, c_2, \dots)$.

2.2 Study of an individual event

From the sample of air showers of interest, each event is to be studied separately. One simulates a number of artificial showers whose E-observables are consistent with the real event and which are initiated by different primaries. To this end, showers with different primary energies are simulated; for each of them, E-observables are reconstructed and compared to their observed values for the real shower. Simulated events are then selected for further study by assigning weights proportional to the estimate of how well their E-observables match the data. It is important to use the same reconstruction procedure as in the analysis of the real data; detailed information about the detector is needed at this point.

Any simplified treatment of the detector (unless quantified to be of negligible effect) would weaken the improvements of the proposed method over previous ones.

For each simulated shower, C-observables are reconstructed, again by the same method as used for processing the real data. For each type of primary particle of interest, the distribution of C-observables of simulated showers selected by E-observables is obtained.

Finally, the C-observables measured for the real event are compared with these simulated distributions to determine the probabilities that the event was initiated by various primaries, given the measured E- and C-observables.

2.3 *Study of an ensemble of events*

One is usually interested in a certain range of real primary energies E_0 (see Appendix A for the summary of our notations). We will refer to this range as $\{E\}$; it may be an interval ($E_1 < E_0 < E_2$) or a half-line ($E_0 > E_1$); in general, the restrictions on the energy may be supplemented by those on the arrival directions if a particular region of the sky is studied.

One then selects the data set to be analyzed. While it should more or less correspond to the energy range of interest in terms of the reconstructed energies, the possibility of incorrect energy reconstruction has to be taken into account and the range of reconstructed energies should preferably be extended. In an ideal case, all events recorded by an experiment should enter the sample, but most of them would contribute to the quantities of interest with almost zero weight.

Each of the individual events in the real sample is to be analyzed as described in Sec. 2.2 but keeping track of the original energy E_0 . Namely, for each event and each primary particle, two distributions are to be obtained for the C-parameters of the simulated events: (i) consistent with the observed one by E-parameters and having thrown energies in the domain of interest, $E_0 \in \{E\}$; and (ii) consistent with the real event by E-parameters and having thrown energies outside the domain of interest, $E_0 \notin \{E\}$. Separate probabilities are to be obtained for the cases (i) and (ii).

This is necessary because we want to constrain primary composition in the given domain of physical energies $\{E\}$, and contamination by showers with energies outside $\{E\}$ should be properly taken into account.

Then, the ensemble of these probabilities obtained for all real events in the sample is subject to combinatoric analysis. As a result, either limits or best-fit parameters of the chemical composition of the primary cosmic-ray flux in the energy domain $\{E\}$ are determined. At this last stage of the procedure one takes into account corrections for the “lost events”. These are possible events with thrown energies $E_0 \in \{E\}$ which however would escape from the sample either because their reconstructed energies differ strongly from E_0 , or because of the event quality cuts.

3 Implementation

In this section, we present a detailed algorithm which can be directly used in the analysis of the real data.

3.1 Study of an individual event

Let us consider a single real event with the reported observed parameters $(E_{\text{obs}}, \mathbf{c}_{\text{obs}})$ and the arrival direction (θ, ϕ) in horizontal coordinates. Hereafter, A denotes possible primary-particle type (for example, $A = p$ refers to primary protons, $A = \text{Fe}$ to iron nuclei and $A = \gamma$ to photons). For each A one is interested in, one generates a library of simulated showers which have:

- (i) primary particle A ;
- (ii) arrival direction (θ, ϕ) (or various arrival directions consistent with (θ, ϕ) within the experimental errors, as discussed in Sec. 2.1);
- (iii) energies E_0 in a relatively wide range around E_{obs} .

The thrown energies E_0 of the simulated showers may be chosen randomly from, e.g., the interval $(0.5E_{\text{obs}}, 5E_{\text{obs}})$ according to $1/E_0$ spectrum. This choice of the spectrum for the library enables one to control shower-to-shower fluctuations at high energies but saves computational time; as we will see below, it is **not** the spectrum of real particles which we assume to be realized in Nature. The interval we quote is indicative and should be adapted for particular events, especially at large zenith angles.

The measurement of E-parameters is subject to statistical errors which are studied by experimental groups in detail. The probability distribution that the primary particle which produced an actual shower with the observed E-parameters equal to E_{obs} would rather produce a shower with these parameters equal to E_{rec} is denoted by $g_E(E_{\text{rec}}, E_{\text{obs}})$. This function is usually determined and published by experimental groups. For instance, for the AGASA experiment $g_E(E_{\text{rec}}, E_{\text{obs}})$ is Gaussian in $\log(E_{\text{rec}}/E_{\text{obs}})$ and the standard deviation of E_{rec} is $\sigma_E \approx 0.25E_{\text{obs}}$ [8]. Hence, in a library of simulated showers to be used in the analysis of a real shower with E-parameters equal to E_{obs} , we assign to each simulated shower a weight

$$w_1 = g_E(E_{\text{obs}}, E_{\text{rec}}) .$$

In principle, this function may depend on the type of a primary, but at this stage we use one and the same g_E for all particles.

We emphasise that the function g_E has nothing to do with physical fluctuations in the shower development, nor with primary- and direction-dependent systematics in the energy reconstruction, but describes instead the resolution power of the installation.

Additionally, one may be interested in studying the energy spectrum different from the one used in the simulations of shower library (it may happen, for instance, that the library was simulated with the $E_0^{-\alpha_{\text{lib}}}$ spectrum with $\alpha_{\text{lib}} = 1$ while one is interested in say $\alpha = 2$ or $\alpha = 2.7$). To reproduce the required thrown energy spectrum, an additional weight

$$w_2 = \left(\frac{E_0}{E_{\text{obs}}} \right)^{\alpha_{\text{lib}} - \alpha} \quad (1)$$

is introduced (instead of E_{obs} in the denominator, any other typical energy scale may be used).

The C-parameters are also reconstructed with some statistical errors. In exactly the same way a shower with measured C-parameters equal to \mathbf{c} could produce detector readings corresponding to \mathbf{c}' . We denote the corresponding probability distribution as

$$g_c(\mathbf{c}', \mathbf{c}).$$

Let us enumerate the showers in the library simulated for a given real event and for a given primary A by $i = 1, \dots, M$. The distribution of the parameters \mathbf{c} for the showers consistent with the real one by E-parameters is given by

$$f_A(\mathbf{c}) = \frac{1}{\mathcal{N}} \sum_{i=1}^M g_c(\mathbf{c}, \mathbf{c}_{iA}) w_{1,iA} w_{2,iA}, \quad (2)$$

where we denoted by $w_{1,iA}$, $w_{2,iA}$ and \mathbf{c}_{iA} the values of the weights and the vector of C-parameters calculated for the simulated shower number i with the primary A , respectively. \mathcal{N} is the normalization factor determined by the condition

$$\int f_A(\mathbf{c}) d\mathbf{c} = 1.$$

By definition, $f_A(\mathbf{c}) d\mathbf{c}$ is the probability to have observed C-parameters in the region $d\mathbf{c}$ centered at \mathbf{c} given the primary particle A and observed E-parameters. This probability assumes that a specific shower-development model used in the simulation code is valid.

To compare the simulated distributions $f_A(\mathbf{c})$ with the observed C-parameters \mathbf{c}_{obs} of the real event, one has to formulate a conjecture about the nature of its primary particle.

One possible question is, how bad the event is described by the primary A – without fixing and studying other possibilities (only the shower library for A

primaries is required in this case). Given the observed values of E_{obs} and \mathbf{c}_{obs} , the event is consistent with the primary A with the probability density

$$\tilde{p}_A = f_A(\mathbf{c}_{\text{obs}}). \quad (3)$$

In the case of practical interest, when the event is unlikely being initiated by the primary A , the estimate of the probability that a given event could be initiated by the primary A is given by

$$p_{A_1} = F_A(\mathbf{c}_{\text{obs}}) \equiv \int_{f_A(\mathbf{c}) \leq f_A(\mathbf{c}_{\text{obs}})} f_A(\mathbf{c}) d\mathbf{c}, \quad k = 1, 2. \quad (4)$$

The use of this estimate is justified if $p_{A_1} \ll 1$.

Another conjecture to be studied might be that the primary was either A_1 or A_2 . In this case, $p_{A_1} + p_{A_2} = 1$ and

$$p_{A_k} = \frac{f_{A_k}(\mathbf{c}_{\text{obs}})}{f_{A_1}(\mathbf{c}_{\text{obs}}) + f_{A_2}(\mathbf{c}_{\text{obs}})}. \quad (5)$$

Clearly, it may happen that the event is poorly described by both A_1 and A_2 , that is $f_{A_1} \approx f_{A_2} \approx 0$ and $p_{A_{1,2}}$ are not stable. This indicates that the conjecture that the primary was either A_1 or A_2 works poorly for this event.

In case one wishes to distinguish between several possible primaries A_1, \dots, A_K , Eq. (5) should be replaced by

$$p_{A_i} = \frac{f_{A_i}(\mathbf{c}_{\text{obs}})}{\sum_{k=1}^K f_{A_k}(\mathbf{c}_{\text{obs}})}.$$

3.2 Study of the ensemble of events

Let us fix the physical energy range $\{E\}$ and consider a sample of N observed events enumerated by $j = 1, \dots, N$, selected as described in Sec. 2.3.

3.2.1 One primary type

To constrain the fraction of the primaries A in the total flux of cosmic-ray particles within the energy domain $\{E\}$, one simulates libraries of A -induced showers described in Sec. 3.1 for each observed event in the sample. When determining the distribution $f_A(\mathbf{c})$, one has to distinguish its two constituents,

$$f_A(\mathbf{c}) = f_A^{(+)}(\mathbf{c}) + f_A^{(-)}(\mathbf{c}), \quad (6)$$

where $f_A^{(+)}(\mathbf{c})$ is the distribution built with only those showers from the library whose thrown energies E_0 belong to the domain $\{E\}$; the rest of showers contribute to $f_A^{(-)}(\mathbf{c})$. Consequently, one obtains for each observed event j , two probabilities:

- $p_A^{(+j)}$, the probability that the event j was initiated by the primary A with energy $E_0 \in \{E\}$; in the case when the event j is unlikely to be induced by primary A , $p_A^{(+j)}$ is given by Eq. (4) with $f_A(\mathbf{c}) = f_A^{(+)}(\mathbf{c})$, otherwise, to get the conservative bound, one can set $p_A^{(+j)} = 1$.
- $p_A^{(-j)}$, the probability that the event j was initiated by the primary A with energy $E_0 \notin \{E\}$; in the case when the event j is unlikely to be induced by primary A , $p_A^{(-j)}$ is given by Eq. (4) with $f_A(\mathbf{c}) = f_A^{(-)}(\mathbf{c})$, otherwise, to get the conservative bound, one can set $p_A^{(-j)} = 0$.

Generally, these two probabilities do not sum up to unity, $p_A^{(+j)} + p_A^{(-j)} < 1$. To proceed further, one needs a conjecture about other possibilities. Namely, we should distinguish between two other probabilities,

- $p_{\bar{A}}^{(+j)}$, the probability that the event j was initiated by any other primary than A with energy $E_0 \in \{E\}$;
- $p_{\bar{A}}^{(-j)}$, the probability that the event j was initiated by any other primary than A with energy $E_0 \notin \{E\}$;

Without assumptions about possible primaries other than A , the two cases $p_{\bar{A}}^{(+j)}$ and $p_{\bar{A}}^{(-j)}$ cannot be distinguished by simulations. A reasonable solution is to assume loosely that the energy was determined correctly by an experiment, $E_0 = E_{\text{rec}}$, and the probability to have the primary energy E_0 follows the distribution $g_E(E_{\text{obs}}, E_0)$. Then,

$$p_A^{(+j)} = \kappa_j \int_{E \in \{E\}} g_E(E_{\text{obs},j}, E) dE, \quad p_A^{(-j)} = \kappa_j \int_{E \notin \{E\}} g_E(E_{\text{obs},j}, E) dE,$$

where the normalisation factor κ_j is determined from the condition

$$p_A^{(+j)} + p_A^{(-j)} + p_{\bar{A}}^{(+j)} + p_{\bar{A}}^{(-j)} = 1.$$

Given the probabilities $p_{A,\bar{A}}^{\pm(j)}$ for each real event j in the sample, one can determine the probability $\mathcal{P}(n_1, n_2)$ to have, among N observed events, n_1 initiated by primaries A with energies $E_0 \in \{E\}$ and n_2 initiated by any other primaries with energies $E_0 \in \{E\}$. We are not interested in what happens outside the domain $\{E\}$, so in what follows we do not distinguish $p_A^{(-j)}$ and $p_{\bar{A}}^{(-j)}$ and use

$$p^{(-j)} \equiv p_A^{(-j)} + p_{\bar{A}}^{(-j)} = 1 - p_A^{(+j)} - p_{\bar{A}}^{(+j)}.$$

The probability $\mathcal{P}(n_1, n_2)$ can be calculated as follows.¹ The probability to have i_1 -th, \dots , i_{n_1} -th observed events (to distinguish them, let us put them in order, $i_1 < \dots < i_{n_1}$) induced by primaries A with $E \in \{E\}$ and k_1 -th, \dots , k_{n_2} -th events ($k_1 < \dots < k_{n_2}$, $i_j \neq k_l$) induced by any other primaries with $E \in \{E\}$ is given simply by the product

$$\mathcal{P}(\{i_j\}, \{k_l\}) = \prod_{i_j} p_A^{(+i_j)} \prod_{k_l} p_{\bar{A}}^{(+k_l)} \prod_{m_n \neq i_j, k_l} p^{(-m_n)}, \quad 1 \leq i_j, k_l, m_n \leq N.$$

To calculate $\mathcal{P}(n_1, n_2)$ one sums over all possible ordered subsets $(\{i_j\}, \{k_l\})$

$$\begin{aligned} \mathcal{P}(n_1, n_2) &= \sum_{\substack{i_1 < i_2 < \dots < i_{n_1} \\ k_1 < k_2 < \dots < k_{n_2}, i_j \neq k_l}} \mathcal{P}(\{i_j\}, \{k_l\}) \\ &= \sum_{\substack{i_1 < i_2 < \dots < i_{n_1} \\ k_1 < k_2 < \dots < k_{n_2}, i_j \neq k_l}} \left[\prod_{i_j} p_A^{(+i_j)} \prod_{k_l} p_{\bar{A}}^{(+k_l)} \prod_{m_n \neq i_j, k_l} p^{(-m_n)} \right], \quad (7) \end{aligned}$$

where $1 \leq i_j, k_l, m_n \leq N$.

Let us suppose now that the fraction of primaries A in the total flux of particles with energies $E_0 \in \{E\}$ is ϵ_A . By definition, ϵ_A is the probability for a single shower with $E_0 \in \{E\}$ to be induced by A , while $(1 - \epsilon_A)$ is a probability for a single shower with $E_0 \in \{E\}$ to be induced by any other primary. Hence $\mathcal{P}(\epsilon)$, the probability that the observed results are reproduced for a given ϵ_A , can be expressed via $\mathcal{P}(n_1, n_2)$ by making use of the formula for a conditional probability,

$$\mathcal{P}(\epsilon_A) = \sum_{n_1, n_2}^{n_1 + n_2 \leq N} \mathcal{P}(n_1, n_2) \epsilon_A^{n_1} (1 - \epsilon_A)^{n_2}. \quad (8)$$

(cf. Ref. [6] for a particular case $n_1 + n_2 = N$). The cases $n_1 + n_2 < N$ reflect the possibility that $N - n_1 - n_2$ events may correspond to primaries with $E_0 \notin \{E\}$.

Making use of the function $\mathcal{P}(\epsilon_A)$, one can constrain the fraction ϵ_A at a given confidence level ξ . Indeed, the allowed region of ϵ_A corresponds to

$$\mathcal{P}(\epsilon_A) \geq 1 - \xi. \quad (9)$$

¹ Alternatively, a simple and fast practical way to determine $\mathcal{P}(n_1, n_2)$ makes use of the Monte-Carlo simulations. One generates a large number of sets of N elements, each element marked either “ $A, E_0 \in \{E\}$ ”, or “ $\bar{A}, E_0 \in \{E\}$ ”, or “ $E_0 \notin \{E\}$ ” with the probabilities $p_A^{(+j)}$, $p_{\bar{A}}^{(+j)}$ and $p^{(-j)}$, respectively (these probabilities are different for different elements $j = 1, \dots, N$). To get $\mathcal{P}(n_1, n_2)$, one simply counts the number of sets with n_1 elements marked “ $A, E_0 \in \{E\}$ ” and n_2 elements marked “ $\bar{A}, E_0 \in \{E\}$ ” and divides this number by the total number of simulated sets.

For sufficiently small values of $p_A^{(+)j}$, the function $\mathcal{P}(\epsilon)$ is a monotonically decreasing function and the allowed region corresponds to $\epsilon_A < \epsilon_0$, where ϵ_0 is determined by $\mathcal{P}(\epsilon_0) = 1 - \xi$; we obtain an upper limit on ϵ_A .

Alternatively, $P(\epsilon_A)$ may be non-monotonic, and the condition (9) may determine one or several intervals allowed for ϵ_A at the confidence level ξ . The most probable value of ϵ_A corresponds to the maximal value of $P(\epsilon_A)$ over $0 \leq \epsilon_A \leq 1$.

Let us remind at this point that if the allowed interval for ϵ_A does not include $\epsilon_A = 0$ at a given C.L., this does not mean we can be sure that there are A -primaries in Nature: this latter statement is true only in the frameworks of the studied hypothesis (primary A versus any other primary with correct energy determination).

The limit one obtains in this way is however biased because some particles with $E_0 \in \{E\}$ may have reconstructed energies so different from E_0 that the corresponding events would not enter the experimental sample chosen for the study. To correct the final result for these “lost” particles, another simulation is required. One should simulate sufficiently large number m of air showers initiated by the primaries A with arrival directions distributed randomly according to the experimental acceptance and energies randomly chosen from the domain $E_0 \in \{E\}$, this time with the realistic spectrum $E_0^{-\alpha}$. Some m_{lost} of these showers will have reconstructed energies E_{rec} (or some other parameters) such that they would escape from the sample chosen for the study; the fraction of these “lost” events is thus $\lambda = m_{\text{lost}}/m$. The true fraction of A -primaries $\epsilon_{A, \text{true}}$ is given by the ratio of the number of A -induced events $M_{A, \text{true}}$ and the sum of the number of these events and the number of events initiated by other particles M ,

$$\epsilon_{A, \text{true}} = \frac{M_{A, \text{true}}}{M_{A, \text{true}} + M}. \quad (10)$$

Similarly, the accessible to our study fraction of A -particles ϵ_A is given by the ratio of accessible to our study fraction of A -induced events $M_A = (1 - \lambda)M_{A, \text{true}}$ and the sum of the number of these events and the number of events initiated by other particles M ,

$$\epsilon_A = \frac{M_A}{M_A + M} = \frac{(1 - \lambda)M_{A, \text{true}}}{(1 - \lambda)M_{A, \text{true}} + M}. \quad (11)$$

Here we assume that other particles do not escape from the sample chosen for the study. Equations (10) and (11) enable one to place a bound on

$$\epsilon_{A, \text{true}} = \frac{\epsilon_A}{1 - \lambda + \lambda\epsilon_A} \quad (12)$$

from previously obtained limit on ϵ_A .

In the energy region to be studied, the expected spectra of different primaries may be different. Corresponding spectral indices may be probed within our approach. Indeed, in the example considered above, $\mathcal{P}(\epsilon_A)$ depends also on the spectral index α_A , Eq.(1). The search for the maximum of $\mathcal{P}(\epsilon_A)$ could be performed with account of this new variable thus revealing, in general, the excluded (or most probable, see sections below) region(s) of (ϵ_A, α_A) parameter space. The extension to several primaries A_1, A_2, \dots is straightforward.

3.2.2 Two or more primary types

Let us turn now to the study of the conjecture that all primary particles in the energy domain $\{E\}$ were either A_1 or A_2 . This requires simulation and processing of the libraries of A_1 - and A_2 -induced showers and no additional assumptions. The distributions $f_{A_1, A_2}^{(\pm)j}(\mathbf{c})$ are obtained for each event j and four probabilities are obtained:

- $p_{A_1}^{(+j)}$ — event j initiated by the primary A_1 with $E_0 \in \{E\}$;
- $p_{A_1}^{(-j)}$ — event j initiated by the primary A_1 with $E_0 \notin \{E\}$;
- $p_{A_2}^{(+j)}$ — event j initiated by the primary A_2 with $E_0 \in \{E\}$;
- $p_{A_2}^{(-j)}$ — event j initiated by the primary A_2 with $E_0 \notin \{E\}$

These probabilities are determined as follows,

$$p_{A_1, A_2}^{(\pm)j} = \frac{f_{A_1, A_2}^{(\pm)j}(\mathbf{c}_{\text{obs}})}{f_{A_1}^{(+j)}(\mathbf{c}_{\text{obs}}) + f_{A_1}^{(-j)}(\mathbf{c}_{\text{obs}}) + f_{A_2}^{(+j)}(\mathbf{c}_{\text{obs}}) + f_{A_2}^{(-j)}(\mathbf{c}_{\text{obs}})}. \quad (13)$$

Now

$$p^{(-j)} = p_{A_1}^{(-j)} + p_{A_2}^{(-j)} = 1 - p_{A_1}^{(+j)} - p_{A_2}^{(+j)} \quad (14)$$

corresponds to the primaries with $E_0 \notin \{E\}$.

The probability $\mathcal{P}(n_1, n_2)$ corresponds now to the case when in the set, n_1 primaries A_1 with $E_0 \in E$, n_2 primaries A_2 with $E_0 \in E$ and $N - n_1 - n_2$ primaries A_1 or A_2 with $E_0 \notin \{E\}$ are present. It is determined by the same Eq. (7) with the replacements $A \rightarrow A_1, \bar{A} \rightarrow A_2$, where $p_{A_1, 2}^{(+j)}$ and $p^{(-j)}$ are now given by Eqs. (13), (14). It also can be determined by the Monte-Carlo simulation described above.

If the fraction of primaries A_1 in the energy domain $\{E\}$ is ϵ_{A_1} , then, within the conjecture we study, the rest $1 - \epsilon_{A_1}$ correspond to A_2 . Thus $P(\epsilon_{A_1})$ is given by the same Eq. (8) and the region of ϵ_{A_1} allowed at the confidence level ξ is again determined by $P(\epsilon_{A_1}) \geq 1 - \xi$.

The most probable value of ϵ_{A_1} may be determined by maximization of $P(\epsilon_{A_1})$.

Account of the “lost” events requires, in this case, determination of two “lost” fractions, λ_{A_1} and λ_{A_2} . From the relation

$$\epsilon_{A_1} = \frac{\epsilon_{A_1}^{\text{true}}(1 - \lambda_{A_1})}{\epsilon_{A_1}^{\text{true}}(1 - \lambda_{A_1}) + (1 - \epsilon_{A_1}^{\text{true}})(1 - \lambda_{A_2})}$$

one obtains

$$\epsilon_{A_1}^{\text{true}} = \frac{\epsilon_{A_1}(1 - \lambda_{A_2})}{1 - \lambda_{A_1} + \epsilon_{A_1}(\lambda_{A_1} - \lambda_{A_2})}. \quad (15)$$

Generalization of the procedure and equations to the case of more than two primary types A_k , $k = 1, \dots, K$, $K > 2$, is straightforward. In particular, one defines the probability to have a set of fractions $(\epsilon_{A_1}, \dots, \epsilon_{A_K})$, $\sum_k \epsilon_{A_k} = 1$, among the primaries with $E_0 \in \{E\}$. The probability $\mathcal{P}(n_1, n_2)$ is now replaced by $\mathcal{P}(n_1, \dots, n_K)$ which can be calculated using a similar method. The function $P(\epsilon_{A_1}, \dots, \epsilon_{A_K})$ can be again expressed via $\mathcal{P}(n_1, \dots, n_K)$ by making use of the formulae for conditional probability,

$$P(\epsilon_{A_1}, \dots, \epsilon_{A_K}) = \sum_{\substack{n_1, \dots, n_K \\ (\sum_i n_i) \leq N}} \mathcal{P}(n_1, \dots, n_K) \cdot \prod_{k=1}^K \epsilon_{A_k}^{n_k}, \quad \sum_{k=1}^K \epsilon_{A_k} = 1.$$

Determination of the best-fit composition would require, in this case, maximization of $P(\epsilon_{A_1}, \dots, \epsilon_{A_{K-1}})$ with respect to $K - 1$ fractions ϵ_k (note that $\epsilon_{A_K} = 1 - \sum_{k=1}^{K-1} \epsilon_{A_k}$).

4 Examples

In this section, we illustrate the method with several simple (toy) examples. For the data, we choose the highest-energy cosmic-ray events reported by the AGASA [9] and Yakutsk [10] experiments (see Table B.1 for the list of events we use and Ref. [4] for more details). The E-observable used by the both experiments is $S(600)$, the signal density at 600 m from the shower core. For a given zenith angle θ , it is in one-to-one correspondence with E_{rec} . Here, we use only one c-observable, $\rho_\mu(1000)$, the muon density at 1000 m from the core. Observed arrival directions, E_{obs} and $\rho_\mu(1000)$ are given in Table B.1 in Appendix B, where we also present technical details of the simulation procedure. The procedure used to reconstruct E_{rec} and $\rho_\mu(1000)$ is described in Appendix C.

We do not discuss many experimental details and the model dependence of the results, so all three examples in this section should be considered as toy ones serving the only purpose to illustrate the method.

4.1 Example 1: an individual event

The procedure described in this section has to be performed for each real event in the dataset. Shower libraries for different primaries are generated as described in Appendix B, and E_{rec} and $\rho_\mu(1000)$ are determined for each simulated shower using the procedure presented in Appendix C. In this example, we consider the highest-energy AGASA event (event 1 from Table B.1).

Simulations of the AGASA detector and the reconstruction procedure [9] indicate that the function g_E is Gaussian in $\log E$ with the width corresponding to the standard deviation of 25% of the central value in terms of energy. This corresponds to $\sigma_l \approx 0.104$ for $\log E$,

$$g_E(E_{\text{obs}}, E_{\text{rec}}) = \frac{1}{\sqrt{2\pi}\sigma_l} e^{-\frac{\log^2(E_{\text{rec}}/E_{\text{obs}})}{2\sigma_l^2}}, \quad \int_0^{+\infty} g_E(E_{\text{obs}}, E_{\text{rec}}) \frac{dE_{\text{rec}}}{E_{\text{rec}}} = 1.$$

Though the detector errors in determination of ρ_μ and fitting the muon LDF may vary with the muon density and number of detectors hit, in our toy example we use for the function g_c the approximation [11] of the Gaussian distribution with the width of 40% of the central value. In our case, there is only one C-observable, $\rho_\mu(1000) \equiv c$, and we thus have

$$g_c(c', c) = \frac{e^{-\frac{(c-c')^2}{2\sigma_c^2}}}{\int_0^\infty e^{-\frac{(c-c')^2}{2\sigma_c^2}} dc}, \quad \sigma_c = 0.4c'.$$

If we are interested in the primary particle of this particular event only, we should use Eq. (2) to determine f_γ , f_p and f_{Fe} . These functions are plotted in Fig. 1. These three functions allow to quantify, in particular, the answers to the questions:

- How bad this event is described by a photon (of any energy), without fixing other possibilities? With the help of Eqs. (3), (4), one finds for this case

$$\tilde{p}_\gamma \approx p_\gamma \approx 0.$$

- Suppose that the event may be initiated either by a photon or by a proton (of any energy). Which primary is preferred? Application of Eq. (5) results in

$$p_\gamma \approx 0.001; \quad p_p \approx 0.999.$$

- Suppose that the event may be initiated either by a proton or by an iron nuclei (of any energy). Which primary is preferred? Application of Eq. (5) results in

$$p_p \approx 0.69; \quad p_{\text{Fe}} \approx 0.31.$$

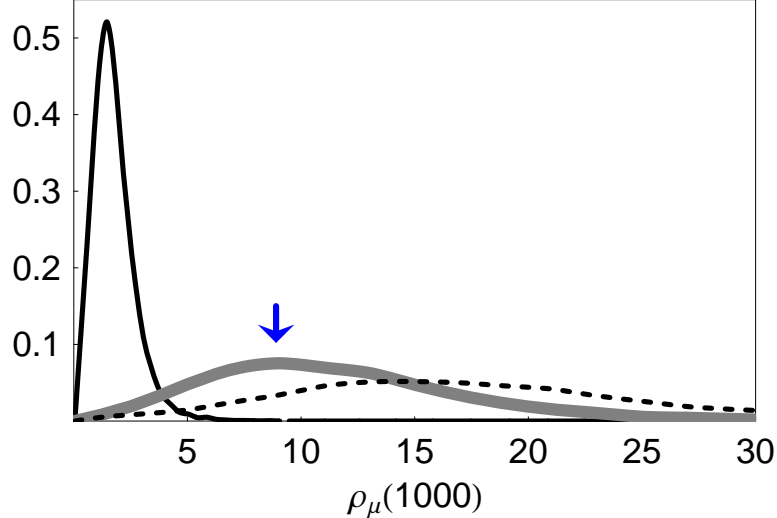


Fig. 1. Distributions of muon densities f_A of simulated events consistent with Event 1 by the arrival direction and the reconstructed energy: thin dark line, $A = \gamma$; thick gray line, $A = p$; dashed line, $A = \text{Fe}$. The arrow indicates the observed value of $\rho_\mu(1000)$ for Event 1.

We emphasise once again that the probability $p_p \approx 1$ in the p - γ comparison does not mean it was surely a proton: this is true only for the hypothesis that either protons or photons can be the primaries. Indeed, $p_p < 1$ for the p -Fe comparison. The difference between protons and iron nuclei is not significant for a single event(cf. Fig. 1). Nevertheless, this difference becomes more pronounced for samples of several events.

We note that the two-primary comparison is complementary to the one-primary analyses because the latter assume correct energy determination for a part of showers (this or any other hypothesis is necessary for obtaining quantitative results).

In the following examples (Sec. 4.2, 4.3), we will study ensembles of events containing this Event 1. Hence we will need the functions $f_A^{(\pm)}$ determined in Eq. (6) for the energy domains $\{E\}$ to be used in these examples: $E_0 \geq 10^{20}$ eV for Example 2 (Sec. 4.2) and $E_0 \geq 1.5 \cdot 10^{20}$ eV for Example 3 (Sec. 4.3). For the latter case, we plot in Fig. 2 functions $f_p^{(\pm)}$; the function $f_p^{(-)}$ corresponds to lower energies and hence lower muon densities. The probabilities $p_\gamma^{(\pm)}$ and $p_\gamma^{(\pm)}$ for the limit on the gamma-ray primaries, $\{E\} = \{E_0 > 10^{20} \text{ eV}\}$, calculated as discussed in Sec. 3.2.1, and probabilities $p_p^{(\pm)}$ and $p_{\text{Fe}}^{(\pm)}$, $\{E\} = \{E_0 > 1.5 \cdot 10^{20} \text{ eV}\}$, calculated with the help of Eq. (13) for the proton-iron discrimination, are presented both for the Event 1 discussed here and for other events in the samples in Tables 1 and 3 in Sec. 4.2 and 4.3, respectively.

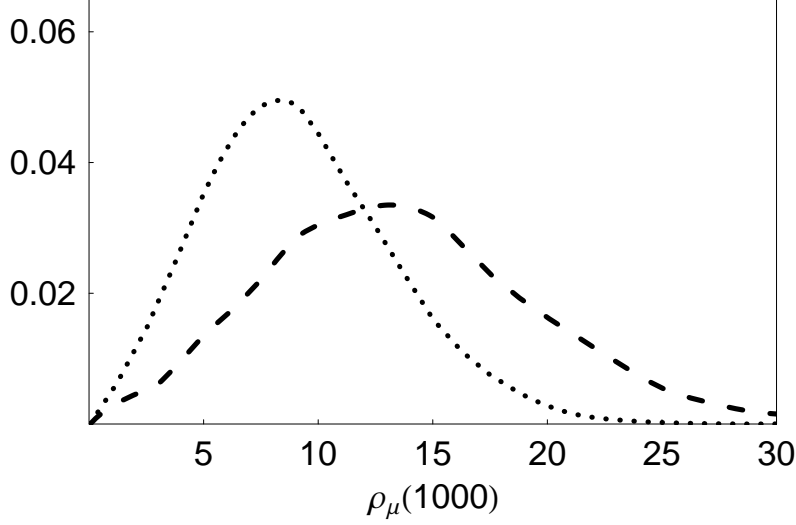


Fig. 2. Distributions of muon densities f_p of simulated proton-induced events consistent with Event 1 by the arrival direction and the reconstructed energy: dotted line, $f_p^{(-)}$ (corresponds to $E_0 < 1.5 \cdot 10^{20}$ eV); dashed line, $f_p^{(+)}$ (corresponds to $E_0 > 1.5 \cdot 10^{20}$ eV).

4.2 Example 2: Limit on the gamma-ray fraction

We concentrate here on obtaining the limit on the gamma-ray primaries with energies $E_0 > 10^{20}$ eV based on the AGASA data. The energy domain of interest is thus $\{E\} = \{E_0 > 10^{20} \text{ eV}\}$. For the experimental sample we take all AGASA events with known muon data and energies $E_{\text{obs}} > 8 \cdot 10^{19}$ eV: this widening of the energy range (cf. Sec. 2.3) compared to the domain $\{E\}$ is justified because photon energies may be estimated incorrectly by the experiment. There are six events in the sample (events 1–6 in Table B.1); see Ref. [4] for the application of the same procedure to a larger dataset supplemented by Yakutsk events. For each of the real events we determine the probabilities $p_{\gamma, \bar{\gamma}}^{(\pm)}$ in the same way as described in Sec. 4.1 for the Event 1. The probabilities are given in Table 1. Corresponding probabilities $\mathcal{P}(n_1, n_2)$ to have n_1 gamma-ray primaries with $E_0 > 10^{20}$ eV and n_2 other primaries with $E_0 > 10^{20}$ eV, calculated as discussed in Sec. 3.2.1, are presented in Table 2.

Figure 3 presents the function $P(\epsilon_\gamma)$ obtained from the values of $\mathcal{P}(n_1, n_2)$ with the help of Eq. (8). It is monotonically decreasing: this reflects the fact that the presence of gamma-ray primaries is disfavoured and the most probable fraction (corresponding to the maximal value of $P(\epsilon_\gamma)$) is $\epsilon_\gamma = 0$. We illustrate Eq. (9) for two confidence levels, $\xi = 0.95$ and $\xi = 0.68$: $\epsilon_\gamma < 0.21$ at 68% C.L. and $\epsilon_\gamma < 0.47$ at 95% C.L.

To account for the “lost photons” whose true energies were $E_0 > 10^{20}$ eV but reconstructed energies were $E_{\text{rec}} < 8 \cdot 10^{19}$ eV, we simulated $m = 1000$

Event	$p_{\gamma}^{(+)}$	$p_{\gamma}^{(-)}$	$p_{\bar{\gamma}}^{(+)}$	$p_{\bar{\gamma}}^{(-)}$
1	0.000	0.000	1.000	0.000
2	0.001	0.000	0.998	0.001
3	0.013	0.003	0.921	0.063
4	0.003	0.000	0.887	0.111
5	0.000	0.000	0.580	0.420
6	0.000	0.000	0.565	0.435

Table 1

Probabilities $p_{\gamma, \bar{\gamma}}^{(\pm)}$ (see text for notations) for individual events 1–6 entering the sample for Example 2 (the limit on the gamma-ray primary fraction with $\{E\} = \{E_0 > 10^{20} \text{ eV}\}$).

	$n_2 = 0$	$n_2 = 1$	$n_2 = 2$	$n_2 = 3$	$n_2 = 4$	$n_2 = 5$	$n_2 = 6$
$n_1=0$	0.000	0.000	0.001	0.036	0.234	0.442	0.268
$n_1=1$	0.000	0.000	0.000	0.005	0.009	0.005	
$n_1=2$	0.000	0.000	0.000	0.000	0.000		
$n_1=3$	0.000	0.000	0.000	0.000			
$n_1=4$	0.000	0.000	0.000				
$n_1=5$	0.000	0.000					
$n_1=6$	0.000						

Table 2

The probabilities $\mathcal{P}(n_1, n_2)$ to have n_1 gamma-ray primaries with $E_0 > 10^{20}$ eV and n_2 other primaries with $E_0 > 10^{20}$ eV in the sample of 6 events used in Example 2. Correct experimental energy determination was assumed for non-photon primaries. Note that $n_1 + n_2 \leq 6$ and the rest $6 - n_1 - n_2$ particles have energies $E_0 < 10^{20}$ eV in each case.

photon-induced showers whose arrival directions were distributed following the AGASA acceptance (with the zenith angle cut of 45°) and energies $E_0 \geq 10^{20}$ eV chosen randomly to follow E_0^{-2} spectrum suggested by several theoretical models with raising super-GZK photon component. The fraction $\lambda \approx 0.035$ of these events had reconstructed energies $E_{\text{rec}} < 8 \cdot 10^{19}$ eV and are therefore “lost”. Application of Eq. (12) results in

$$\epsilon_{\gamma, \text{true}} < 0.22 \quad \text{at } 68\% \text{ C.L.},$$

$$\epsilon_{\gamma, \text{true}} < 0.50 \quad \text{at } 95\% \text{ C.L.}$$

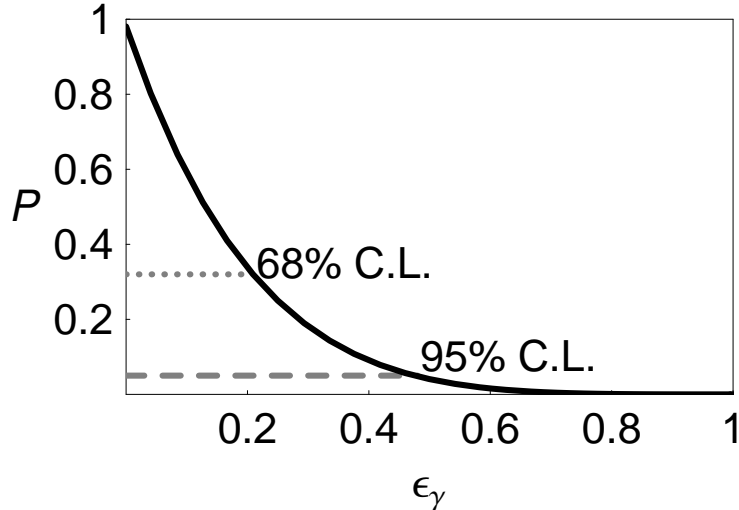


Fig. 3. $P(\epsilon_\gamma)$ calculated for the Example 2. Dashed line corresponds to $1 - P = 0.95$ (the 95% C.L. upper limit on ϵ_γ), dotted line – to $1 - P = 0.68$ (the 68% C.L. upper limit).

Event	$p_p^{(+)}$	$p_p^{(-)}$	$p_{\text{Fe}}^{(+)}$	$p_{\text{Fe}}^{(-)}$
1	0.254	0.445	0.136	0.165
2	0.295	0.349	0.135	0.221
7	0.163	0.001	0.735	0.101
8	0.407	0.107	0.256	0.230

Table 3

Probabilities $p_{p,\text{Fe}}^{(\pm)}$ (see text for notations) for individual events 1, 2, 7, 8 entering the sample for Example 3 (comparison of protons and iron nuclei).

4.3 Example 3: Favoured hadronic composition

To illustrate the case when two possible primary types are compared, we consider four events with $E_{\text{obs}} > 1.5 \cdot 10^{20}$ eV and known muon content (two observed by AGASA and two by Yakutsk; events 1, 2, 7 and 8 from Table B.1). The primary composition in the domain $\{E\} = \{E_0 > 1.5 \cdot 10^{20}$ eV} will be constrained within the hypothesis that the primaries are either protons or iron nuclei.

In a way similar to Sec. 4.1, we process all four events and obtain probabilities $p_{p,\text{Fe}}^{(\pm)}$, Eq. (13), which are listed in Table 3. They are transformed into probabilities $\mathcal{P}(n_1, n_2)$ to have n_1 proton primaries with $E_0 > 1.5 \cdot 10^{20}$ eV and n_2 iron primaries with $E_0 > 1.5 \cdot 10^{20}$ eV among the four events we discuss (see Table 4). The function $P(\epsilon_p)$, plotted in Fig. 4, looks quite different from $P(\epsilon_\gamma)$ from the previous example. There is no clear preference of either proton

	$n_2 = 0$	$n_2 = 1$	$n_2 = 2$	$n_2 = 3$	$n_2 = 4$
$n_1=0$	0.012	0.102	0.110	0.035	0.003
$n_1=1$	0.044	0.226	0.138	0.020	
$n_1=2$	0.057	0.149	0.041		
$n_1=3$	0.028	0.030			
$n_1=4$	0.005				

Table 4

The probabilities $\mathcal{P}(n_1, n_2)$ to have n_1 proton primaries with $E_0 > 1.5 \cdot 10^{20}$ eV and n_2 iron primaries with $E_0 > 1.5 \cdot 10^{20}$ eV in the sample of 4 events used in Example 3. Note that $n_1 + n_2 \leq 4$ and $4 - n_1 - n_2$ particles have energies $E_0 < 1.5 \cdot 10^{20}$ eV in each case.

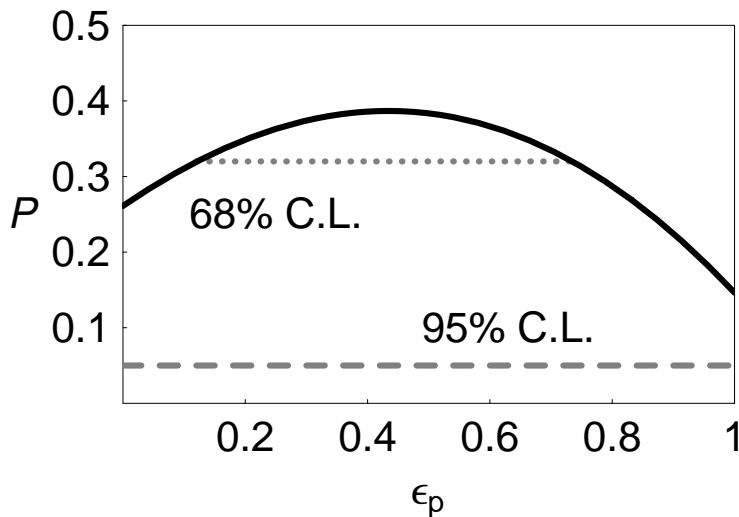


Fig. 4. $P(\epsilon_p)$ calculated for the Example 3. Notations are the same as in Fig. 3

or iron primaries, and the function has a wide bump. The maximum corresponds to the most probable proton fraction $\epsilon_p \sim 0.39$, but at the 95% C.L., the proton fraction is unconstrained. Clearly, the main reason for the weakness of the constraint is the small number of events in the sample. The limit at the 68% C.L. illustrates the situation expected at higher confidence level for larger samples: the constraint reads $0.12 < \epsilon_p < 0.73$. It is reassuring that with only four events and for such a difficult task as to distinguish between different hadronic primaries, our method still allows to obtain some indicative information: heavier composition is slightly preferred.

A minor additional complication in this example, as compared to the Example 2, relates to the calculation of the fractions of “lost” particles. The reason is that we unified data from two experiments in a single sample. We suppose that both experiments have similar sensitivities to different primaries (otherwise the unification of data sets would not be justified anyway). Then the

expected total number of events which may be observed by an experiment is proportional to its exposure. We denote by $\epsilon_p^{\text{true}(I)}$ and $\epsilon_p^{\text{true}(II)}$ the proton fraction calculated with the help of Eq. (15) for the experiments I and II whose exposures are a_I and a_{II} , respectively. The fraction ϵ_p estimated for the combined dataset is then

$$\epsilon_p^{\text{true}} = \frac{\epsilon_p^{\text{true}(I)}}{1 + a_{(II)}/a_I} + \frac{\epsilon_p^{\text{true}(II)}}{1 + a_I/a_{(II)}}.$$

From the simulation of 1000 proton-induced and 1000 iron-induced showers from various arrival directions for each of the two cases – (I) AGASA, $\theta < 45^\circ$, and (II) Yakutsk, $\theta < 60^\circ$ – one obtains $\lambda_p^{(I)} \approx 0.05$, $\lambda_{\text{Fe}}^{(I)} \approx 0.06$, $\lambda_p^{(II)} \approx 0.11$, $\lambda_{\text{Fe}}^{(II)} \approx 0.08$. Since λ_p and λ_{Fe} are relatively close to each other, their contributions balance each other in Eq. (15), and the resulting limits on ϵ_p^{true} do not differ from the limits on ϵ_p without the correction for “lost” events (clearly, this would not be so in a general case).

4.4 Testing the method with artificial samples

To test how well the method works, we perform analyses similar to those of Sec. 4.1–4.3 but for a simulated data sample with known primaries. To this end, we generated showers with the arrival directions of events 1–8 (this allowed us to use the shower libraries generated for examples 1–3 above) and kept record of their primary particles and E_0 . For each shower, we reconstructed $S(600)$ (and hence E_{rec}) and $\rho_\mu(1000)$ taking into account random detector errors. Then, we performed our analyses and compared their results with known primary content of the fake sample.

The events of the simulated sample are listed in Table B.2. For the study similar to Sec. 4.2, we take events F1–F6 of which three are initiated by protons and three by photons (that is, $\epsilon_\gamma = 0.5$). Individual probabilities $p_\gamma, p_{\bar{\gamma}}$ for these events are given in Table 5. Application of the method gives, at the 95% C.L., $\epsilon_\gamma < 0.73$ if we take the sample with $E_{\text{obs}} \geq 0.9 \cdot 10^{20}$ eV and $\epsilon_\gamma < 0.72$ if we use only five events with $E_{\text{obs}} \geq 10^{20}$ eV (the difference in the fractions of lost photons compensates the difference in statistics).

For a study similar to Example 2, we take four events (F1, F2, F7 and F8) of which two are initiated by protons and two by iron nuclei, that is $\epsilon_p = 0.5$. The probabilities $P_{p,\text{Fe}}^{(\pm)}$ are given in Table 6. The most favoured composition is obtained to be $\epsilon_p \approx 0.45$, but any is allowed at the 95% C.L.

Event	$p_{\gamma}^{(+)}$	$p_{\gamma}^{(-)}$	$p_{\bar{\gamma}}^{(+)}$	$p_{\bar{\gamma}}^{(-)}$
F1	0.000	0.000	1.000	0.000
F2	0.000	0.000	0.993	0.007
F3	0.391	0.287	0.130	0.192
F4	0.000	0.000	0.887	0.113
F5	0.150	0.534	0.258	0.058
F6	0.273	0.090	0.630	0.007

Table 5

Probabilities $p_{\gamma,\bar{\gamma}}^{(\pm)}$ (see text for notations) for individual events F1–F6 entering the artificial sample for the limit on the gamma-ray primary fraction with $\{E\} = \{E_0 > 10^{20} \text{ eV}\}$.

Event	$p_p^{(+)}$	$p_p^{(-)}$	$p_{\text{Fe}}^{(+)}$	$p_{\text{Fe}}^{(-)}$
F1	0.281	0.084	0.450	0.184
F2	0.159	0.421	0.086	0.333
F7	0.159	0.064	0.300	0.476
F8	0.458	0.070	0.323	0.149

Table 6

Probabilities $p_{p,\text{Fe}}^{(\pm)}$ (see text for notations) for individual events F1, F2, F7, F8 entering the artificial sample for comparison of protons and iron nuclei.

5 Conclusions

To summarise, we presented a simple method which allows to improve precision of the studies of the primary composition of ultra-high-energy cosmic rays. Each event is studied individually. The simulated showers are selected by the physical observables to be consistent with the real event.

Our approach exploits the fact that the uncertainty in discrimination of the primary-particle types by conventional methods is determined not only by intrinsic fluctuations of the shower development, but also by the spread related to the arrival direction. Averaging over arrival directions introduces artificial, easy-to-avoid, fluctuations in the determination of both the reconstructed energy (see Fig. 5 for an illustration) and composition-related parameters (Fig. 6).

While the direction-related systematical effects are controlled within our method, there are still many other sources of uncertainty, the most important among them are the low precision of the measurement of composition-related quantities in experiments and artificial fluctuations in simulated air showers due to

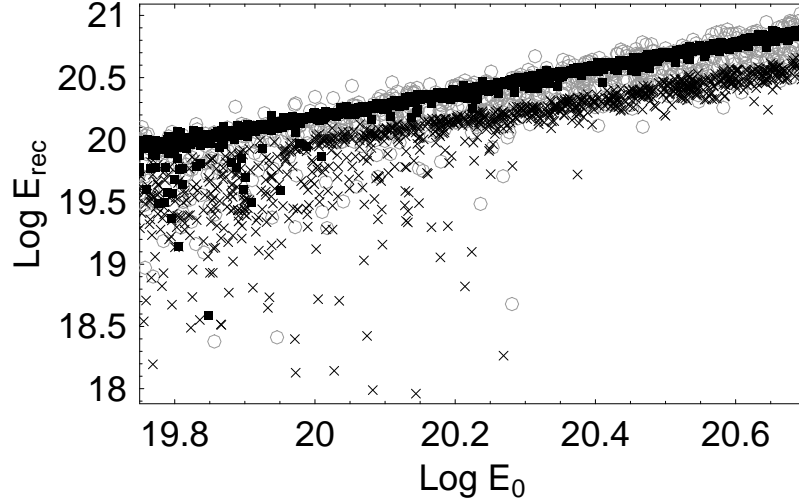


Fig. 5. Direction dependence of the reconstructed energy for gamma-ray primaries. Plotted is the reconstructed energy (determined by the AGASA method from $S(600)$) versus the primary energy. Dark boxes: arrival direction of the event 1; crosses: arrival direction of the event 3; grey circles: arrival directions randomly distributed according to the AGASA acceptance ($0 < \theta < 45^\circ$). Both E_0 and E_{rec} are measured in eV.

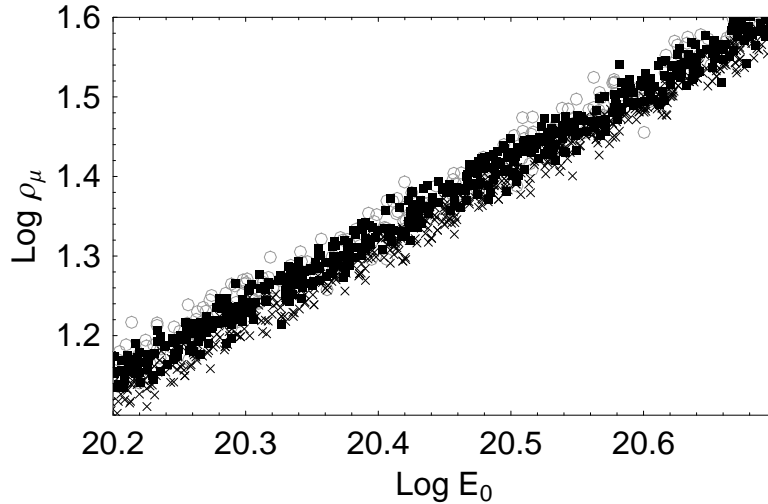


Fig. 6. Direction dependence of muon density for iron primaries. Plotted is $\rho_\mu(1000)$ versus the primary energy. Dark boxes: arrival direction of the event 7 ($\theta \approx 48^\circ$); crosses: arrival direction of the event 8 ($\theta \approx 59^\circ$); grey circles: arrival directions randomly distributed according to the Yakutsk acceptance ($0 < \theta < 60^\circ$). E_0 is measured in eV, ρ_μ is measured in m^{-2} .

use of the thinning approximation. Use of multiple c -observables, their careful choice and optimisation of simulations may help to improve further the precision of our method.

As for any other method based on air-shower simulations, the capabilities of our approach are limited (and severely limited in the case of distinguish-

ing different hadronic primaries) because of persistent theoretical problems in modelling high-energy hadronic interactions.

As compared to the traditional methods, the event-by-event study requires more computational time, which makes it difficult to implement it for large samples in the form described here. However, almost the same level of precision may be reached with reasonable binning in zenith (and in some cases also azimuth) angle.

As we have seen in Sec. 4, the method is really strong in studies of the small samples, notably for the highest-energy or somewhat special (e.g. correlated with particular hypothetical sources) events, where statistics is insufficient to obtain confident conclusions with the help of traditional methods. In some cases, e.g. to constrain the gamma-ray primaries, even a single event may be successfully studied.

Acknowledgements

We are indebted to L. Dedenko, M. Kachelrieß, M. Pravdin, K. Shinozaki, D. Semikoz and M. Teshima for numerous helpful discussions. This work was supported in part by the INTAS grant 03-51-5112, by the Russian Foundation of Basic Research grants 05-02-17363 (DG and GR) and 04-02-17448 (DG), by the grants of the President of the Russian Federation NS-7293.2006.2 (government contract 02.445.11.7370; DG, GR and ST) and MK-2974.2006.2 (DG), by the fellowships of the "Dynasty" foundation (awarded by the Scientific Council of ICFPM, DG and GR) and of the Russian Science Support Foundation (ST). Numerical part of the work was performed at the computer cluster of the Theoretical Division of INR RAS.

A Notations

A : the index enumerating different primaries, $A = p, \text{ Fe}, \gamma, \dots$

\bar{A} : denotes any other primary but A .

$\mathbf{c} = (c_1, c_2, \dots)$ – the set of c -observables (observables used to distinguish different primaries). \mathbf{c}_{obs} denotes the values of these observables for a particular real event.

E-observables – the observables used for the energy estimation.

E_0 – the real energy of the primary particle; for simulated events it is the parameter of the simulation.

E_{rec} – the reconstructed energy of a simulated shower; it is an E-observable (in the sense that it is in one-to-one correspondence with the observable used to estimate the energy for a given arrival direction) and can be determined for each air shower according to the reconstruction procedure fixed by the experiment (see Appendix C). In general, $E_{\text{rec}} \neq E_0$ due to both statistical and systematic errors.

E_{obs} – the reported energy of a given observed air shower.

$\{E\}$ – the region of primary energies E_0 for which the composition is to be constrained.

ϵ_A – the fraction of the primaries A in the total flux of cosmic rays with energies $E_0 \in \{E\}$.

$\epsilon_{A,\text{true}}$ – the fraction ϵ_A corrected for the “lost events”.

λ – the fraction of the “lost events”, that is of the showers whose primaries had the energies $E_0 \in \{E\}$ but which did not enter the sample because of incorrect energy determination.

B Observed and simulated events used in examples

Experimental information required for the simulations in Examples 1–3 of Sec. 4 is taken from Refs. [4,9,10] and is summarised in Table B.1.

The artificial events F1–F8 used in examples of Sec. 4.4 have the same arrival directions and experimental conditions as the corresponding events 1–8 and are listed in Table B.2.

For each of the eight events, we generated libraries of simulated showers induced by primaries required for the particular examples (see column (8) of Table B.1). For each observed event and each primary, 1000 showers were generated. Thrown energies E_0 of the simulated showers were randomly selected between 5×10^{19} eV and 5×10^{20} eV following the spectrum E_0^{-1} , as discussed in Sec. 3.1. The arrival directions of the simulated showers were the same as those of the corresponding real events. The simulations were performed with CORSIKA v6.204 [12], choosing QGSJET 01c [13] as high-energy and FLUKA 2003.1b [14] as low-energy hadronic interaction model. Electromagnetic showering was implemented with EGS4 [15] incorporated into CORSIKA. Possible interactions of the primary photons with the geomagnetic field

No.	Exp.	E_{obs}	θ	ϕ	$\rho_{\mu}^{\text{obs}}(1000)$	Examples	Simulated
(1)	(2)	(3)	(4)	(5)	(6)	(7)	(8)
1	AGASA	2.46	36.5	79.2	8.9	1,2,3	γ, p, Fe
2	AGASA	2.13	22.9	55.5	10.7	2,3	γ, p, Fe
3	AGASA	1.44	14.2	27.5	8.7	2	γ
4	AGASA	1.34	35.1	234.9	5.9	2	γ
5	AGASA	1.05	33.7	291.6	12.6	2	γ
6	AGASA	1.04	35.6	100.0	9.3	2	γ
7	Yakutsk	1.60	47.7	180.8	19.6	2,3	p, Fe
8	Yakutsk	1.50	58.7	230.6	11.8	2,3	p, Fe

Table B.1

Events analysed in examples in Sec. 4.1–4.3. The columns give (1) reference number, (2) experiment name (which determines the conditions for simulations), (3) the reported energy in units of 10^{20} eV, (4) and (5) horizontal coordinates in degrees (azimuth angle $\phi = 0$ corresponds to a particle coming from the South, $\phi = 90^\circ$ – from the West), (6) reported muon density at 1000 m from the core in units of m^{-2} , (7) numbers of examples in Sec. 4 where this event is used, (8) types of primary particles of simulated showers.

No.	primary	E_0	E_{obs}	$\rho_{\mu}^{\text{obs}}(1000)$
(1)	(2)	(3)	(4)	(5)
F1	p	1.78	2.45	17.7
F2	p	1.55	1.84	10.9
F3	γ	1.05	0.94	1.0
F4	p	1.04	1.35	13.1
F5	γ	1.03	1.25	1.0
F6	γ	1.21	1.77	1.8
F7	Fe	1.65	2.10	14.9
F8	Fe	2.69	1.71	20.7

Table B.2

Artificial events analysed in examples in Sec. 4.4. The columns give (1) reference number, (2) primary particle, (3) the original energy in units of 10^{20} eV, (4) the reconstructed energy in units of 10^{20} eV, and (5) reconstructed muon density at 1000 m from the core in units of m^{-2} .

were simulated with the PRESHOWER option of CORSIKA [16]. As suggested in Ref. [17], all simulations were performed with thinning level 10^{-5} , maximal weight 10^6 for electrons and photons, and 10^4 for hadrons.

For each simulated shower, we determined $S(600)$ and $\rho_\mu(1000)$. The plane orthogonal to the arrival direction has been divided into concentric rings of the width of 100 m; contributions of all particles were averaged over these rings to reconstruct the lateral distribution function. For the calculation of the signal density, we used the detector response functions from Refs. [18,19]. The reconstructed energy – the E-observable which we compared to the experimental values – was obtained by making use of exactly the same procedure as used in processing the real data; see Appendix C.

C Reconstruction of energy and muon density

It is important to process the simulated events in a way as close as possible to the procedure with which the observables we use were obtained for the real events. For completeness, we recall here the relevant procedures for AGASA and Yakutsk.

C.1 AGASA energy estimation

For the primary energy estimation, AGASA used the following procedure (the Takeda method, Ref. [8]).

The lateral distribution function (LDF) of the signal is obtained by fitting the scintillator detectors' readings by the empirical formula [20],

$$S(r) \propto \left(\frac{r}{R_M}\right)^{-1.2} \left(1 + \frac{r}{R_M}\right)^{-(\eta-1.2)} \left(1 + \left(\frac{r}{R_1}\right)^2\right)^{-0.6},$$

where

$$\eta = 3.97 - 1.79(\sec \theta - 1), \quad R_M = 91.6 \text{ m}, \quad R_1 = 1000 \text{ m}$$

and r denotes the distance to the shower core. Only detectors with $300 \text{ m} \leq r \leq 1000 \text{ m}$ are used for the fit. $S(600)$ is the value of the fitted LDF at $r = 600 \text{ m}$.

Due to the 10% one-side systematic error reported in Ref. [8], the value of $S(600)$ observed by AGASA is larger than the real one by a factor of 1.1 which should be taken into account for the simulated events:

$$S_{\text{AGASA}}^\theta(600) = 1.1 S^\theta(600)$$

The energy estimation formula is [21]

$$E = 2.03 \cdot 10^{17} \text{ eV } S_{\text{AGASA}}^0(600),$$

where $S^0(600)$ is the signal density for a vertical shower related to the real density of an inclined shower $S_{\text{AGASA}}^\theta(600)$ by the attenuation formula [20]

$$S_{\text{AGASA}}^\theta(600) = S_{\text{AGASA}}^0(600) \exp\left(-\frac{X_0}{\Lambda_1}(\sec\theta - 1) - \frac{X_0}{\Lambda_2}(\sec\theta - 1)^2\right),$$

where

$$X_0 = 920 \text{ g/cm}^2, \quad \Lambda_1 = 500 \text{ g/cm}^2, \quad \Lambda_2 = 594 \text{ g/cm}^2$$

The simulations should be performed for the AGASA atmospheric depth, $X_{\text{AGASA}} \approx 960 \text{ g/cm}^2$ (note that $X_{\text{AGASA}} \neq X_0$).

C.2 AGASA muon density estimation

AGASA detects the number of muon-counter hits, which is expected to be equal to the number of muons with kinetic energy $E_{\text{kin}} > 0.5 \text{ GeV}/\cos\theta_\mu$, where θ_μ is the zenith angle of a particular muon.

To determine the muon density at 1000 m from the core, the densities measured by the detectors between 800 m and 1600 m from the core are fitted by the empirical LDF [22]

$$\rho_\mu(r) \propto \left(\frac{r}{R_0}\right)^{-0.75} \left(1 + \frac{r}{R_0}\right)^{-\beta} \left(1 + \left(\frac{r}{R_1}\right)^3\right)^{-\delta},$$

where

$$\beta = 2.52, \quad \delta = 0.6, \quad R_0 = 266 \text{ m}, \quad R_1 = 800 \text{ m}.$$

The value of the fitted LDF at $r = 1000 \text{ m}$, $\rho_\mu(1000)$, is used as the primary composition estimator.

C.3 Yakutsk energy estimation

The energy estimation in the Yakutsk array [23,24] is quite similar to that of AGASA. The value of $S(600)$ is determined by fitting the scintillator detectors' readings by the following empirical formula,

$$S(r) \propto \left(\frac{r}{R_M}\right)^{-a} \left(1 + \frac{r}{R_M}\right)^{a-b} \left(1 + \left(\frac{r}{R_1}\right)\right)^{-g},$$

where ²

$$R_M = 68.0 \text{ m}, \quad R_1 = 2000 \text{ m}, \quad a = 1.3, \quad b = 3.24 - 2.6(1 - \cos \theta), \quad g = 3.5.$$

The attenuation formula is

$$S(600) = S^0(600) \left((1 - \beta) \exp \left(-\frac{X_0}{\Lambda_E} (\sec \theta - 1) \right) + \beta \exp \left(-\frac{X_0}{\Lambda_M} (\sec \theta - 1) \right) \right).$$

The energy conversion formula is

$$E = 4.6 \cdot 10^{17} \text{ eV} \left[S^0(600) \right]^{0.98},$$

where

$$X_0 = 1020 \text{ g/cm}^2, \quad \Lambda_E = 250 \text{ g/cm}^2, \quad \Lambda_M = 2500 \text{ g/cm}^2, \quad \beta = 0.39 \cdot \left[S^0(600) \right]^{-0.12}.$$

The simulations are to be performed for the Yakutsk atmospheric depth, $X_{\text{Yakutsk}} = X_0 \approx 1020 \text{ g/cm}^2$.

C.4 Yakutsk muon density estimation

For the two events we use, the Yakutsk muon detectors counted muons with $E_{\text{kin}} > 1.0 \text{ GeV} / \cos \theta_\mu$.

To apply one and the same procedure to both AGASA and Yakutsk results, we use the muon density at 1000 m as the parameter to be compared with simulations. The Yakutsk muon detectors have larger area and significantly higher saturation threshold than AGASA's, so the detector readings in a wider region, 400 m to 2000 m, are used in the LDF fit by the following empirical formula [26,23]

$$\rho_\mu(r) \propto \left(\frac{r}{R_0} \right)^{-0.75} \left(1 + \frac{r}{R_0} \right)^{0.75 - b_\mu} \left(1 + \frac{r}{R_1} \right)^{-g_\mu},$$

where $R_0 = 280 \text{ m}$, $R_1 = 2000 \text{ m}$, $g_\mu = 8$ and b_μ , together with the overall proportionality coefficient, is a free fitting parameter.

² The actual procedure is more involved[25]. It takes into account the atmospheric conditions at the arrival time of a given event, that in particular results in an event dependence of R_M which varies usually within $60 \text{ m} < R_M < 80 \text{ m}$. The detector responses then are adjusted in order to get the same energy estimate with $R_M = 68.0 \text{ m}$, that allows to treat the data uniformly. Since this procedure adopted by Yakutsk collaboration is unambiguos, our simple method is justified.

References

- [1] M. T. Dova, A. G. Mariazzi and A. A. Watson, arXiv:astro-ph/0512408.
- [2] B. McBreen and C. J. Lambert, Phys. Rev. D **24** (1981) 2536.
- [3] E. E. Antonov *et al.*, JETP Lett. **68**, 185 (1998) [Pisma Zh. Eksp. Teor. Fiz. **68**, 177 (1998)]; M. Ave, R. A. Vazquez and E. Zas, Astropart. Phys. **14**, 91 (2000).
- [4] G. I. Rubtsov *et al.*, Phys. Rev. D **73** (2006) 063009 [arXiv:astro-ph/0601449].
- [5] F. Halzen, R. A. Vazquez, T. Stanev and H. P. Vankov, Astropart. Phys. **3** (1995) 151.
- [6] P. Homola *et al.*, Nucl. Phys. B (Proc. Suppl.) **151** (2006) 116; M. Risse *et al.*, Phys. Rev. Lett. **95** (2005) 171102.
- [7] M. Risse *et al.*, Nucl. Phys. Proc. Suppl. **151**, 96 (2006); M. Risse *et al.*, Astropart. Phys. **21**, 479 (2004).
- [8] M. Takeda *et al.*, Astropart. Phys. **19**, 447 (2003).
- [9] N. Hayashida *et al.*, astro-ph/0008102, see also <http://www-akeno.icrr.u-tokyo.ac.jp/AGASA/>.
- [10] V. Egorova *et al.*, Nucl. Phys. Proc. Suppl. **136**, 3 (2004); M.I. Pravdin, Proc. 29th ICRC (Pune), 2005; S. P. Knurenko *et al.* astro-ph/0411683.
- [11] K. Shinozaki *et al.*, Astrophys. J. **571**, L117 (2002).
- [12] D. Heck *et al.*, Report FZKA-6019 (1998), Forschungszentrum Karlsruhe
- [13] N. N. Kalmykov, S. S. Ostapchenko and A. I. Pavlov, Nucl. Phys. Proc. Suppl. **52B**, 17 (1997).
- [14] A. Fassó, A. Ferrari, P. R. Sala, in Proc. of the MonteCarlo 2000 Conference, A. Kling *et al.* (eds.), p. 159-164 (Springer Berlin 2001); A. Fassó *et al.*, *ibid.* p. 955.
- [15] W. R. Nelson, H. Hirayama, D.W.O. Rogers, SLAC-0265
- [16] P. Homola *et al.*, Comp. Phys. Comm. **173** (2005) 71.
- [17] M. Kobal *et al.*, Astropart. Phys., **15**, 259 (2001).
- [18] N. Sakaki *et al.*, Proc. ICRC 2001, **1**, 333.
- [19] L. G. Dedenko *et al.*, Nucl. Phys. Proc. Suppl. **136**, 12 (2004).
- [20] S. Yoshida *et al.*, J. Phys. G **20** (1994) 651.
- [21] H. Y. Dai *et al.*, J. Phys. G **14** (1988) 793.
- [22] N. Hayashida *et al.*, J. Phys. G **21** (1995) 1101.

- [23] A. V. Glushkov *et al.*, Phys. Atom. Nucl. **63**, 1477 (2000) [Yad. Fiz. **63** (2000) 1557].
- [24] M. Pravdin *et al.* in Proc. of 29th ICRC, Pune, India (2005) v.7, 243-246.
- [25] N. N. Efimov *et al.*, in Catalogue of HECR N3, World Data Center C2, Japan (1988).
- [26] A. V. Glushkov *et al.*, JETP Lett. **71**, 97 (2000) [Pisma Zh. Eksp. Teor. Fiz. **71** (2000) 141].